# A REDUCED DEGREE OF FREEDOM MODEL FOR THERMAL PERMEABILITY ENHANCEMENT IN BLOCKY ROCK

## D. ELSWORTH* and J. XIANG

*Department of Mineral Engineering, The Pennsylvania State University,
University Park, PA 16802, U.S.A.*

**Abstract**—An upwind-weighted finite-element model is presented for the analysis of non-boiling hot dry rock geothermal systems. The model accommodates the essential mechanisms of permeability enhancement or degradation resulting from injection of fluid at a temperature different from ambient. The effects of induced thermal strains and fluid pressures in conditioning both normal and shear displacements in an ubiquitously jointed continuum are accommodated. The mass is idealized as a blocky assemblage where diffusive-advective energy transport in the fracture system is augmented by transient heat supply from intact rock blocks. The true transient nature of both energy supply from the blocks to the percolating fluid and the development of thermal strains within the medium are determined analytically. The local assumption of full lateral restraint coupled with analytical representation of thermal strains renders the nonlinear initial-value problem fully defined in terms of the two dependent variables of fluid pressure and fluid temperature only. Subject to these assumptions, complete fluid-pressure and fluid-temperature histories of large, thermally stimulated reservoirs may be determined effectively and efficiently. Results are presented for both single point injection and dual point injection-withdrawal scenarios to illustrate the possible scope of the method.

## NOMENCLATURE

| | |
|---|---|
| $a$ | block radius |
| $a_f$ | fracture area (per unit volume) |
| $A_1, A_2$ | block displacement coefficients |
| $B_1, B_2$ | block flux coefficients |
| $D, \mathbf{D}$ | thermal conductivity, conductivity matrix |
| $E$ | modulus of elasticity |
| $\mathbf{E}$ | advective transport matrix |
| $f_s$ | block surface heat flux |
| $\mathbf{F}$ | fluid heat capacity matrix |
| $G$ | shear modulus |
| $\mathbf{G}$ | solid heat capacity matrix |
| $\mathbf{H}$ | fluid thermal expansion matrix |
| $k_n, k_s$ | rock joint normal and shear stiffnesses |
| $K, \mathbf{K}$ | hydraulic conductivity, conductivity matrix |
| $l$ | summation integer (time step) |
| $n$ | summation integer |
| $P, \mathbf{P}$ | fluid pressure, nodal fluid pressure vector |
| $q_e, q_s$ | external hydraulic flux, block thermal flux |
| $\mathbf{q}_f, \mathbf{q}_s$ | nodal fluid discharge vector, nodal thermal discharge vector |
| $r$ | radial coordinate |
| $S$ | joint shear strength (effective stress) |
| $\mathbf{S}$ | fluid storativity matrix |
| $t, \Delta t$ | time and time increment |
| $T, \mathbf{T}$ | temperature, nodal temperature vector |
| $T_r, T_a$ | block temperatures at radii r and a |
| $u_a, u_r$ | block surface displacement, block radial displacement (spherical block) |

* Currently at, Waterloo Centre for Groundwater Research, University of Waterloo, Waterloo, Ontario, N2L 3G1, Canada.

| $u_b$ | block surface displacement (prismatic block) |
| $x_i$ | Cartesian coordinates |
| $\alpha$ | coefficient of thermal expansion |
| $\beta$ | compressibility |
| $\phi$ | porosity |
| $\phi_b, \phi_d$ | joint friction angle, joint dilation angle |
| $\lambda, \mu$ | Lamé coefficients |
| $\nu$ | Poisson ratio |
| $\rho c$ | specific heat capacity |
| $\gamma$ | unit weight |
| $\sigma_{ij}$ | in-situ stresses |
| $\Delta\sigma_{ij}$ | change in joint normal ($i = j$) and shear ($i \neq j$) stress |
| $\Delta\sigma_{ij}^s$ | change in joint normal stress (dilation) |

*Subscripts*
| f | fluid |
| s | solid |

*Superscripts*
| t | time |
| . | time derivative |

## INTRODUCTION

Permeability changes that occur in competent, blocky rock under non-isothermal fluid injection have been well documented (Murphy, 1982). The process is particularly evident in hot dry rock (HDR) geothermal energy schemes where permeability enhancement is effected by the complex interaction of injected fluid pressures and induced thermal stresses. Increased *fluid pressures* within a minimally permeable and initially fractured rock mass result in joint opening (Brekke *et al.*, 1972; Noorishad *et al.*, 1984), shear deformation and bridging (Pine and Cundall, 1985) and, under more extreme conditions, crack extension (Fairhurst, 1964). Since the fluid permeability of single fractures is proportional to aperture raised to the power three, small dilatant deformations may greatly increase formation permeability (Elsworth and Goodman, 1985). Sudden, non-uniform or cyclic *temperature changes* may overstress the intact rock and result in increased fracture density of cracks at the micro- and macro-scales (Nemat-Nasser, 1982). Additionally, *transient cooling* of the rock mass induces contractile volumetric strains that may generate an increase in pre-existing macro-fracture volume, even in the absence of new crack formation. The behavior of the reservoir under this mode of thermal loading is determined primarily by the redistribution of thermal strains and in-situ stresses that result from quenching. Transient reduction of flow impedance within reservoirs producing at quasi-constant rate is most likely attributed to these multiple interacting phenomena.

The following addresses a simplified treatment of the behavior of an HDR reservoir containing a pre-existing ubiquitous, orthogonal fracture system. The treatment describes the transient development of rock-joint deformations that result from changes in fluid pressure and thermal straining within an initially stressed formation. The initial assumption is that the jointed rock mass may be represented as a two-phase continuum comprising solid rock blocks separated by fluid-filled discontinuities. Advective transport operates within the pre-existing fracture system with conductive transfer being the dominant mechanism governing thermal transfer between non-porous rock blocks and the fracture fluid.

Rock-mass displacements and stresses are not explicitly accommodated. Rather, transient thermal volumetric strains are evaluated under the assumption that a macroscopic control volume containing an assemblage of rock blocks will remain at constant volume. Volume changes are therefore restricted to within the solid phase. For both heat production from the intact rock blocks and volumetric deformation of the mass an analytical transfer function is used to accurately gauge the unsteady behavior and determine the magnitude of permeability

enhancement. This representation allows the behavior of the system to be evaluated with reduced unknowns. The necessary system variables are the transient fluid pressure, rock and fluid temperatures and cartesian displacements within the mass. The assumption of a constant macroscopic control volume eliminates the necessity of recording displacements explicitly and therefore removes the three displacement degrees of freedom from the system. The use of an analytical transfer function documenting the release of thermal energy from the rock blocks similarly allows the rock temperature to be neglected as a degree of freedom. The remaining degrees of freedom comprise fluid pressure and fluid temperature, only. The desire in reducing the degrees of freedom to this level is to allow large simulations to be efficiently completed while still representing the major interacting components of the system.

## MODEL ASSUMPTIONS

The following assumptions are germane to the reduced degree of freedom representation:

(1) The dominant energy transport modes are conduction within the solid phase and mixed advection and diffusion within the fracture system.

(2) Changes in fracture aperture may result from fluid pressure transients, thermal strains and shear displacement.

(3) A constant control volume and assumptions consistent with full lateral restraint of the control volume are imposed.

(4) The load-deformation behavior of component fractures is trilinear in normal closure and linear in shear deformation. At failure, the fractures are purely frictional with a constant angle of dilation.

For HDR geothermal energy recovery, induced advective transport is the primary mode of heat transfer. Continuing microseismic activity and reduction of flow impedance with time are two factors that suggest aperture enhancement as the predominant mechanism by which permeability of the mass increases under steady production.

## SYSTEM EQUATIONS

Two coupled partial differential equations govern the performance of the saturated rock system. Transient solution for mass balance provides the requisite pressure distribution which, in turn, controls thermal dissipation through advective flow. The mass balance and energy balance equations relevant to an ubiquitously jointed and initially isothermally saturated rock mass are, respectively

$$\frac{\partial}{\partial x_i}\left(\frac{K_f}{\gamma_f}\frac{\partial P_f}{\partial x_j}\right) + \rho_f q_e = \phi\beta_f\frac{\partial P_f}{\partial t} - \phi\alpha_f\frac{\partial T_f}{\partial t} \tag{1}$$

$$\frac{\partial}{\partial x_i}\left(\frac{D_f}{\phi}\frac{\partial T_f}{\partial x_j}\right) - \rho_f c_f\left(\frac{q_f}{\phi}\right)_i\frac{\partial T_f}{\partial x_i} + q_s = \rho_f c_f\frac{\partial T_f}{\partial t} \tag{2}$$

where subscript f denotes fluid parameters, subscript s denotes terms pertaining to the solid (rock) phase and; $T_f$ = fluid temperature, $P_f$ = fluid pressure, $K_f$ = hydraulic conductivity of fracture system, $D_f$ = thermal conductivity of fluid, $c_f$ = specific heat capacity of fluid, $q_e$ = externally supplied hydraulic flux (injection or withdrawal rates), $q_f$ = total hydraulic flux (per unit volume), $\rho_f$ = fluid density, $\gamma_f$ = fluid unit weight, $\phi$ = fracture porosity of ubiquitously jointed mass, $\beta_f$ = fluid compressibility, $\alpha_f$ = coefficient of thermal expansion of the fluid, $q_s$ = thermal flux from solid phase (per unit volume), and $x_i$ = cartesian coordinate where, in general, i = 1, 3. Two dimensional analysis (i = 1, 2) is considered throughout the following.

The equations are coupled through the magnitude of the advective heat flux term of equation

(2). This is directly dependent on the solution of equation (1). Flow within the rock mass is controlled by temperature dependent fluid viscosity. The ability of single fractures to transmit fluid is strongly controlled by the fracture aperture (b).

Although not explicitly represented in the heat transport or flow equations, changes in fracture apertures may be effected by either modification of the fluid pressure regime or as the result of thermal straining within the matrix blocks. The effects of fluid pressures and thermal strains on the stress and displacement regime at the block surfaces may be accommodated under the assumption of full lateral restraint. Under this assumption, displacements between adjacent fracture walls may be determined directly from the known fluid pressures present within the fracture network and from the calculated thermal history at block faces, only. If the thermal history of fluid temperature at individual block faces may be determined, the induced thermal stress and thermal displacement histories may also be uniquely evaluated.

## ANALYTICAL TRANSFER FUNCTIONS

Two transfer functions are required to supplement equations (1) and (2). The first is to represent the thermal contraction or expansion of individual blocks under a changing surface temperature regime. This displacement will directly affect the magnitude of the hydraulic conductivity term $(K_f)$ in equation (1). The second transfer function is required to accurately describe the thermal flux stimulated from the block as it is cooled or warmed from ambient temperature. This thermal energy will be transferred directly to the advecting fluid through $q_s$ in equation (2). To maintain the problem definition at a tractable level, individual rock blocks are represented as equivalent spheres. This concept together with the rock mass geometry is illustrated in Fig. 1.

### Block surface displacement
For an unstressed spherical block of radius a, coefficient of thermal expansion $\alpha_s$ and with a radial temperature distribution within the solid material $T_r$, the displacement at any radius r may be given as (Boley and Weiner, 1960)

$$u_r = \alpha_s \left( \frac{3\lambda + 2\mu}{\lambda + 2\mu} \right) \left\{ \frac{1}{r^2} \int_0^r T_r r^2 \, dr + \frac{4\mu}{(3\lambda + 2\mu)} \left( \frac{r}{a^3} \right) \int_0^a T_r r^2 \, dr \right\} \tag{3}$$
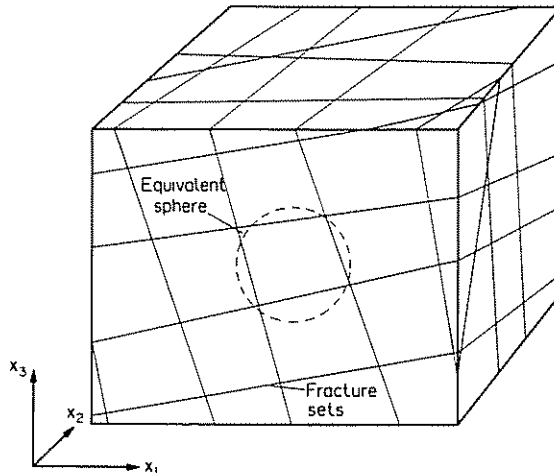


Fig. 1. Geometry of an ubiquitously jointed mass showing actual prismoidal and idealized spherical blocks.

where $\lambda$ and $\mu$ are Lamé coefficients. Although, in general, the temperature distribution within the block is a complex function of the external thermal loading history, the only specific interest in the context of this work is the boundary displacement at $r = a$. This displacement controls volumetric strain within the fractured medium. The block surface displacement, $u_a$, is therefore

$$u_a = \frac{3\alpha_s}{a^2} \int_0^a T_r r^2 \, dr \qquad (4)$$

which, in a thermally equilibrated block at constant radial temperature $T_r$ above initial ambient, results in a surface displacement of $u_a = \alpha_s T_r a$.

The temporal and spatial variation in temperature within a spherical block, warmed or cooled at the boundary from ambient temperature may be obtained by solving the spherically symmetric initial value problem subject to the boundary conditions

$$T_r = 0 \qquad\qquad a > r > 0 \text{ for } t = 0^- \qquad (5)$$

$$T_r = T_a \qquad\qquad r = a \text{ for } t > 0^+ \qquad (6)$$

Solution is available as (Carslaw and Jaeger, 1959)

$$T_r^t = T_a + \frac{2aT_a}{\pi r} \sum_{n=1}^{\infty} \frac{(-1)^n}{n} \sin\left(\frac{n\pi r}{a}\right) \exp\left(-D_s n^2 \pi^2 t / \rho_s c_s a^2\right) \qquad (7)$$

where $D_s$ = solid phase thermal conductivity, $\rho_s$ = solid phase density, $c_s$ = solid phase specific heat capacity and the temperatures are determined at all radial locations $(r)$ and for all times $(t)$. Substituting equation (7) into equation (4) and performing the integration yields

$$u_a^t = \alpha_s a T_a \left\{ 1 - \frac{6}{\pi^2} \sum_{n=1}^{\infty} \frac{1}{n^2} \exp\left(-D_s n^2 \pi^2 t / \rho_s c_s a^2\right) \right\} \qquad (8)$$

to give $u_a^t$ = block surface displacement at time t resulting from a step temperature change $(T_a)$ applied at the outer boundary. This may be represented in dimensionless form as illustrated in Fig. 2 to give the block response as a unique function of dimensionless time $D_s t / \rho_s c_s a^2$. For a continuously varying applied thermal boundary condition $(T_a^t)$ the time dependent surface displacement may be obtained from use of a convolution product via Duhamel's Theorem (Carslaw and Jaeger, 1959).
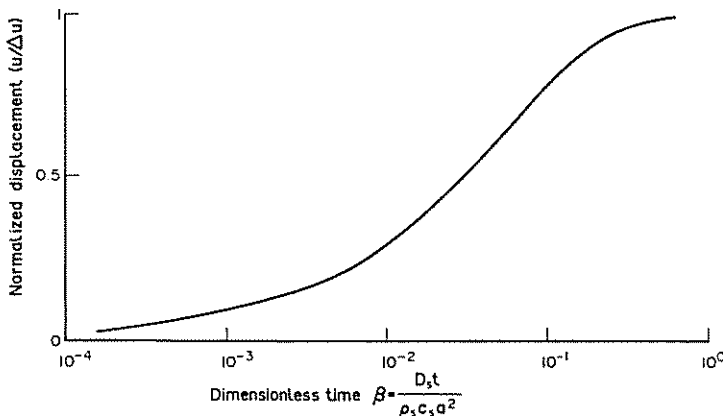


Fig. 2. Dimensionless displacement of an unstressed spherical block with dimensionless time.

Simply stated, this is an application of linear superposition of known thermal boundary conditions with time to yield displacement response. Since

$$u_a^l = f(T_a, t) \tag{9}$$

then by Duhamel's theorem

$$u_a^l = \int_0^t \frac{\partial}{\partial t} f(T_a, t - \tau) \, d\tau \tag{10}$$

or for the specific case of equation (8)

$$u_a^l = \alpha_s a \int_0^t \frac{\partial T_a}{\partial t} \left\{ 1 - \frac{6}{\pi^2} \sum_{n=1}^{\infty} \frac{1}{n^2} \exp\left(\xi(t - \tau)\right) \right\} d\tau \tag{11}$$

where

$$\xi = -D_s n^2 \pi^2 / \rho_s c_s a^2$$

In general, the variation of temperature will not be known as a continuous function of time but will be evaluated only at the close of finite time increments $\Delta t$. Finite representation of the partial differential of equation (11) yields a series expansion

$$u_a^{l=l+1} \cong \alpha_s a \frac{\Delta T_a^1}{\Delta t^1} \int_{t_0}^{t_1} \left\{ 1 - \frac{6}{\pi^2} \sum_{n=1}^{\infty} \frac{1}{n^2} \exp\left(\xi(t^{l+1} - \tau)\right) \right\} d\tau$$

$$+ \alpha_s a \frac{\Delta T_a^2}{\Delta t^2} \int_{t_1}^{t_2} \left\{ 1 - \frac{6}{\pi^2} \sum_{n=1}^{\infty} \frac{1}{n^2} \exp\left(\xi(t^{l+1} - \tau)\right) \right\} d\tau$$

$$+ \cdots + \alpha_s a \frac{\Delta T_a^{l+1}}{\Delta t^{l+1}} \int_{t^l}^{t^{l+1}} \left\{ 1 - \frac{6}{\pi^2} \sum_{n=1}^{\infty} \frac{1}{n^2} \exp\left(\xi(t^{l+1} - \tau)\right) \right\} d\tau \tag{12}$$

with

$$\frac{\Delta T_a^{l+1}}{\Delta t^{l+1}} = \frac{T_a^{l+1} - T_a^l}{t^{l+1} - t^l} \tag{13}$$

Performing the integration of equation (12) at the two time steps of $t^l$ and $t^{l+1}$ allows the displacement at the latter time level ($u_a^{l+1}$) to be evaluated from the displacement at the previous time level ($u_a^l$). This is determined by the relation

$$u_a^{l+1} = A_1^{l+1} + A_2^{l+1} \tag{14}$$

$$A_1^{l+1} = A_1^l + a\alpha_s \Delta T^{l+1} \tag{15}$$

$$A_2^{l+1} = \sum_{n=1}^{\infty} A_2^l \exp\left(\xi \Delta t^{l+1}\right) + a\alpha_s \frac{\Delta T^{l+1}}{\Delta t^{l+1}} \frac{6}{\pi^2} \sum_{n=1}^{\infty} \frac{1}{n^2 \xi} \left(1 - \exp\left(\xi \Delta t^{l+1}\right)\right) \tag{16}$$

Surface displacement may be determined for any quantified history of surface temperatures in a sphere initially at a datum temperature.

*Block surface heat flux*

A similar procedure to the previous may be followed to determine heat flux transfer (Bibby,

1981; Huyakorn *et al.*, 1983) from the surface of the spherical blocks as a function of time. Solution of the spherical heat flow, initial value problem is reported in equation (7). Thermal flux $(f_s)$ at the sphere boundary is given as

$$f_s = -D_s \frac{\partial T}{\partial r}\bigg|_{r=a} \tag{17}$$

which on substituting equation (7) yields flux per unit surface area as

$$f_s = -\frac{2D_s T_a}{a} \sum_{n=1}^{\infty} \exp{(\xi t)} \tag{18}$$

The flux per unit volume $(q_s)$ is given as

$$q_s = f_s \times \frac{4\pi a^2}{(4/3)\pi a^3} = f_s \times \frac{3}{a} \tag{19}$$

which on substitution into Duhamel's Theorem of equation (10) yields the volumetric rate of heat production $(q_s)$ as

$$q_s^{l+1} = B_1^{l+1} \Delta T^{l+1} + B_2^{l+1} \tag{20}$$

$$B_1^{l+1} = \frac{6D_s}{a^2 \Delta t^{l+1}} \sum_{n=1}^{\infty} \frac{1}{\xi} \{1 - \exp{(\xi \Delta t^{l+1})}\} \tag{21}$$

$$B_2^{l+1} = \sum_{n=1}^{\infty} q_s^l \exp{(\xi \Delta t^{l+1})} \tag{22}$$

It must be observed that both the displacement $(u_a)$ and heat flux $(q_s)$ terms are functions of infinite exponential series. The convergence of these series are particularly poor for small values of the coefficient $D_s \Delta t / \rho_s c_s a^2$. If, however, the time step increment $(\Delta t)$ is retained constant then the terms of the exponential series of equations (16), (21) and (22) are also constant with time and need only be evaluated once. More onerous than this is the requirement that the values of $A_2^l$ (equation 16) and $B_2^l$ (equation 22) are stored for each spatial evaluation of $u_a^l$ or $q_s^l$ and for each of the n terms of the truncated series.

*Induced thermal porosity change*

For considerations of equivalent total thermal energy it is necessary that the idealized spherical block and real cubic rock block illustrated in Fig. 1 have identical volumes. Consider a rock mass with ubiquitous orthogonal joint sets of uniform spacing (s) and hence frequency of 1/s. The equivalent spherical radius $(a)$ may be equated as

$$a = \left(\frac{3}{4\pi}\right)^{1/3} s \tag{23}$$

For infinitesimal radial displacement on the surface of this sphere of $(\Delta u)$ the resulting volumetric strain $(\Delta v/v)$ of the sphere and hence the rock mass is obtained from the corollary of equation (19) and equation (23) as

$$\frac{\Delta v}{v} = \frac{-3\Delta u_a}{a} = \frac{-3}{s}\left(\frac{4\pi}{3}\right)^{1/3} \Delta u_a \tag{24}$$

where contractile strains, compressive stresses and outward radial displacements are defined positive.

In a cooling block, deformations are uniformly distributed within the three orthogonal directions. Contractile volume strain may, therefore, be distributed equally between aperture enlargements on joint sets normal to the orthogonal axes. Total fracture area ($a_f$) in a control volume $dx_i$ on edge is

$$a_f = \frac{3}{s}\, dx_1\, dx_2\, dx_3 \tag{25}$$

and therefore the potential change in aperture ($\Delta u_j$) will be

$$\Delta u_j = -\frac{\Delta v}{v}\frac{dx_1\, dx_2\, dx_3}{a_f} \tag{26}$$

On substituting equations (24) and (25) into (26), the potential aperture change ($\Delta u_j$) is

$$\Delta u_j = \left(\frac{4\pi}{3}\right)^{1/3}\Delta u_a \cong 1.612\Delta u_a \tag{27}$$

This gives the potential for aperture enhancement ($\Delta u_j$) of existing fractures in an initially *unstressed* medium. For a rock mass under an initial triaxial stress state $\sigma_{ii}$, as illustrated in Fig. 1, displacements induced by changes in joint fluid pressure ($\Delta p$) or changes in thermal stress ($\Delta \sigma_T$) will be moderated by both the in-situ stress field and nonlinear joint stiffness. Assuming a trilinear compression curve for the joint in compression, as illustrated in Fig. 3, and enforcing full lateral restraint, joint opening ($\Delta u_j = -ve$) that results from a change in pressure ($\Delta p$) is given by

$$\Delta u_j = -\left[\frac{E}{s(1-2v)} + k_n\right]^{-1}\Delta p \tag{28}$$

where $k_n$ = joint normal stiffness as defined in Fig. 3 and $s \gg b$. Fluid pressure is assumed to act uniformly on all faces of the block.

For the non-isothermal case, block surface displacements ($\Delta u_b$) and joint displacements ($\Delta u_j$) are clearly related if it is mandated that the control volume ($dx_1\, dx_2\, dx_3$) remain constant. Thus,
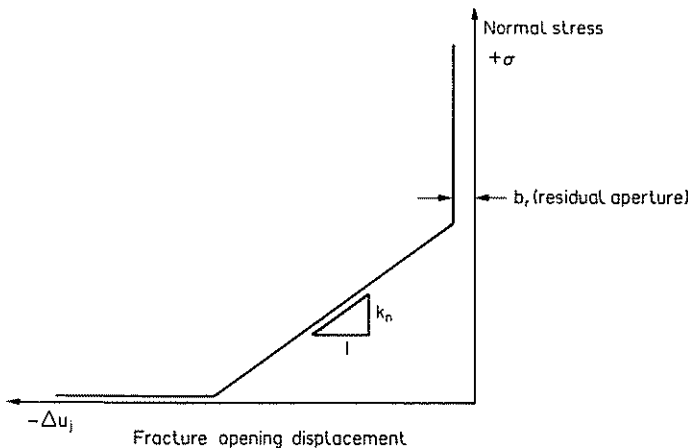


Fig. 3. Trilinear compression curve for a single rock joint in stress-displacement space.

for compatibility

$$\Delta u_b + \Delta u_j = 0 \tag{29}$$

where

$$\Delta u_b = \frac{s(1 - 2v)}{E} \Delta \sigma_{ii} - s a_s \Delta T \tag{30}$$

$$\Delta u_j = \frac{1}{k_n} \Delta \sigma_{ii} \tag{31}$$

and $\Delta \sigma_{ii}$ = change in normal stress due to thermal effects. Noting that $a_s \Delta T = -1/3(\Delta v/v)$, substituting equation (24) into (30) and the result, together with (31) into (29) gives

$$\Delta \sigma_{ii} = \left[ \frac{1}{k_n} + \frac{s(1 - 2v)}{E} \right]^{-1} \left( \frac{4\pi}{3} \right)^{1/3} \Delta u_a \tag{32}$$

Changes in normal stress ($\Delta \sigma_{ii}$) will directly regulate the magnitude of dilational displacements along joint sets. Shear strength ($S$), if assumed to be stress level independent, is given as

$$S = (\sigma_{ii} + \Delta \sigma_{ii} - \Delta P_f) \tan (\phi_b + \phi_d) \quad i = 1, 2 \tag{33}$$

where $\phi_b$ and $\phi_d$ represent angle of frictional resistance and dilation angle, respectively. Changes in shear stress ($\Delta \sigma_{12}$) are directly precipitated by reduction in normal stresses.

The in-situ shear stress from the previous iteration in time ($\sigma_{12}$) is modified according to the available in-situ normal effective stress. The drop in shear stress ($\Delta \sigma_{12}$) that results from a change in normal stress ($\sigma_{ii}$) is represented as

$$\begin{aligned} \Delta \sigma_{12} &= \sigma_{12} - S \quad \text{for} \quad \sigma_{12} > S \\ \Delta \sigma_{12} &= 0 \quad\quad\quad \text{for} \quad \sigma_{12} \leqslant S \end{aligned} \tag{34}$$

The potential for shear displacement $\Delta v_j$ between two blocks follows as

$$\Delta v_j = \left[ \frac{1}{k_s} + \frac{s}{G} \right] \Delta \sigma_{12} \tag{35}$$

where $k_s$ is the linear joint shear stiffness and $G$ the shear modulus of the intact rock. Any shear displacement is moderated by stress buildup that results from joint dilation. Assuming dilation occurs instantaneously with shear initiation, then it follows from equation (28) that

$$\Delta \sigma_{ii}^s = \left[ \frac{E}{s(1 - 2v)} + k_n \right] |\Delta v_j| \tan \phi_d \tag{36}$$

where $\Delta \sigma_{ii}^s$ is the change in normal stress resulting from shear displacement. Considering that, for the failure condition ($\sigma_{12} > S$) the appropriate constitutive relation must hold, then

$$(\sigma_{12} - \Delta \sigma_{12}) = (\sigma_{ii} + \Delta \sigma_{ii} + \Delta \sigma_{ij}^s - \Delta P_f) \tan (\phi_b + \phi_d) \tag{37}$$

which on substituting equations (32), (35) and (36) into (37) gives directly the equilibrium shear stress drop ($\Delta \sigma_{12}$) and consequently the equilibrium shear disaplacement $\Delta v_j$ induced for component thermal displacements ($\Delta u_a$) and changes in fluid pressure ($\Delta_p$). Normal aperture enhancement is evaluated as

$$\Delta u_j = \left[ \frac{E}{s(1 - 2v)} + k_n \right]^{-1} (-\Delta P_f + \Delta \sigma_{ii}^s + \Delta \sigma_{ii}) \tag{38}$$

from which current aperture (b) may be readily determined for any combination of stress level and appropriate joint normal stiffness ($k_n$) such that $b = b_r + \Delta u_j$. With the fissure apertures uniquely defined as functions of thermally induced displacements ($u_a^t$), virgin field stresses ($\sigma_{ii}$), fracture spacing (s), rock mass elastic constants ($E$, $\nu$, $k_n$, $k_s$) and residual apertures ($b_r$) the hydraulic conductivity of the system may be evaluated. Choosing the parallel plate analogy without modification for fracture wall roughness, the hydraulic conductivity of an ubiquitously jointed medium of fracture aperture ($b_j$) is

$$K_{f_i} = \frac{gb_j^3}{6\nu_f s} \quad i = 1, 3; \quad j = 1, 3; \quad i \neq j \tag{39}$$

where $\nu_f$ = fluid kinematic viscosity and g = gravitational acceleration. This completes the definition of all factors strongly influencing the flow regime.

Of all the parameters required to execute an analysis, those describing the nature and separation of the fracture sets are most difficult to determine. Fracture stiffnesses, spacings, frictional characteristics and initial apertures are very difficult to determine, in reality, and must be the object of sensitivity studies if realistic results are to be matched and ultimately projected. The thermal and mechanical parameters describing both the percolating fluid and the intact rock are more narrowly defined and may readily be determined from tabulated values.

## FINITE ELEMENT FORMULATION

The governing partial differential equations may be solved most conveniently by using a finite element scheme. This method allows spatial changes in fracture density and characteristics to be readily accommodated. Normal Galerkin weighting is applied to the mass balance equation (equation 1) and upstream weighting (Christie *et al.*, 1976) is applied to the energy balance equation (equation 2). Analysis by this procedure is well known and will not be further described here. Equations (1) and (2) may be defined, respectively, at the local elemental scale as

$$\mathbf{KP}_f^t + \mathbf{S\dot{P}}_f^t = \mathbf{q}_f^t + \mathbf{H\dot{T}}_f^t \tag{40}$$

$$[\mathbf{D} + \mathbf{E}]\mathbf{T}_f^t + \mathbf{F\dot{T}}_f^t = \mathbf{Gq}_s^t \tag{41}$$

where $\mathbf{K}$ = fluid conductivity matrix, $\mathbf{S}$ = fluid storativity matrix (lumped), $\mathbf{D}$ = thermal diffusion matrix, $\mathbf{E}$ = thermal advection matrix, $\mathbf{F}$ = thermal heat capacity matrix (consistent), $\mathbf{G}$ = rock thermal capacity matrix (consistent), $\mathbf{H}$ = fluid thermal expansion matrix (lumped), $\mathbf{P}_f$ = nodal fluid pressure vector, $\mathbf{q}_f$ = nodal fluid discharge vector, $\mathbf{T}_f$ = nodal fluid temperature vector, $\mathbf{q}_s$ = nodal thermal discharge vector. A dot superscript represents time derivative and both equations are written at time level t as denoted by the superscript. For completeness, the form of the individual matrices representing a four noded element are included in Appendix I. All integrals are determined analytically.

Nodal variables for sequential time steps $t^l$ and $t^{l+1}$ may be written using finite differences via a Crank–Nicolson implicit scheme for equations (40) and (41) where

$$\mathbf{P}_f^{l+\frac{1}{2}} = \tfrac{1}{2}(\mathbf{P}_f^l + \mathbf{P}_f^{l+1}) \tag{42}$$

and

$$\mathbf{T}_f^{l+\frac{1}{2}} = \tfrac{1}{2}(\mathbf{T}_f^l + \mathbf{T}_f^{l+1}) \tag{43}$$

Substituting equations (42), (43) and (20) into equations (40) and (41) and rearranging yields the final system of equations,

$$\left[\frac{1}{2}\mathbf{K}(\mathbf{T_f}) + \frac{1}{\Delta t}\mathbf{S}\right]\mathbf{P}^{l+1} = \left[\frac{1}{\Delta t}\mathbf{S} - \frac{1}{2}\mathbf{K}(\mathbf{T_f})\right]\mathbf{P}^{l} + \frac{1}{2}[\mathbf{q}_f^{l} + \mathbf{q}_f^{l+1}] - \frac{1}{\Delta t}\mathbf{H}[\mathbf{T}^{l+1} - \mathbf{T}^{l}] \tag{44}$$

and

$$\left[\frac{1}{2}(\mathbf{D} + \mathbf{E}) + \frac{1}{\Delta t}\mathbf{F} - \frac{1}{2}\mathbf{GB}_1^{l+1}\right]\mathbf{T}_f^{l+1} = \left[\frac{1}{\Delta t}\mathbf{F} - \frac{1}{2}(\mathbf{D} + \mathbf{E}) + \frac{1}{2}\mathbf{G}(\mathbf{B}_1^{l} - \mathbf{B}_1^{l+1})\right]\mathbf{T}_f^{l}$$
$$- \frac{1}{2}\mathbf{GB}_1^{l}\mathbf{T}_f^{l-1} + \frac{1}{2}\mathbf{G}[\mathbf{B}_2^{l} + \mathbf{B}_2^{l+1}] \tag{45}$$

where hydraulic conductivity $\mathbf{K}(T_f)$ is temperature history dependent. It follows directly from equation (20) that vectors $\mathbf{B}_1$ and $\mathbf{B}_2$ are written to represent nodal magnitudes. These coupled equations are solved iteratively within each time step to describe thermal porosity changes within the formation.

## VALIDATION STUDY

The capabilities of the upwind-weighting scheme used in the finite element formulation have been well demonstrated'in cases where advective transport processes dominate. The dominance of advective transport over diffusive transport is best referenced with respect to the Peclet number $(P_c)$ where, at the local element level,

$$P_c = \frac{q_f l \rho_f c_f}{\phi D_f} \tag{46}$$

and $l$ is the element length. For cases where matrix thermal diffusion is neglected, a comparison of the numerical scheme with the results from an analytical solution (Bear, 1972) and those of other upwind weighted schemes (Noorishad and Mehran, 1982) are illustrated in Fig. 4. Even for the relatively high Peclet number of 100 the numerical results show minimal overshoot, undershoot and smearing of the thermal front.

Where thermal diffusion into the surrounding rock mass (initially at a temperature of zero) is accommodated, the sharpness of the thermal front is diffused. This effect is also illustrated in Fig. 4, where the effects of three different fracture spacings are examined. As would be expected, where the dimensions of individual blocks are small, the rapidity with which the
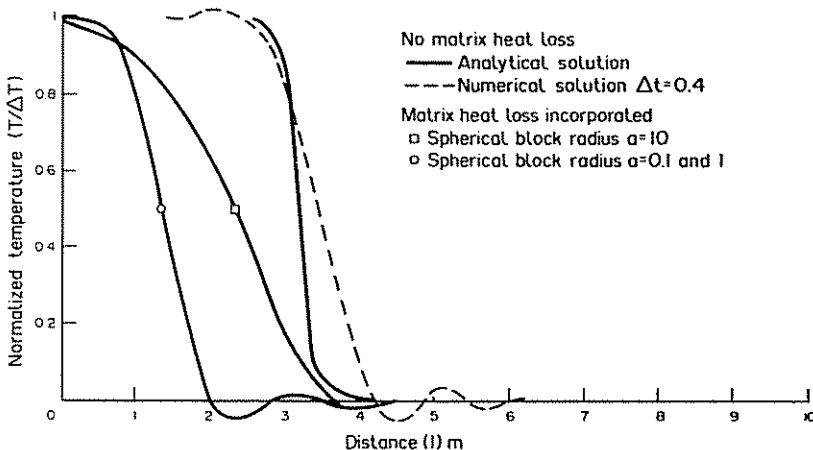


Fig. 4. Validation results for linear flow at a Peclet number (Pc) of 100.

percolating fluid is cooled is most marked. This is due to both the high specific surface area ratio of the smaller blocks and the short heat transfer length afforded by the blocks. Although, from Fig. 4, it is evident that the larger blocks are less efficient in cooling the passing fluid in the short term, the extended duration of the block thermal flux maintains inlet fluid temperatures lower for large blocks versus the smaller blocks.

## PARAMETRIC STUDIES

Two studies are completed to illustrate the system behavior that develops for flow within a two-dimensional section where a cooling fluid is injected into the initially saturated mass.

### Case one

The first is for a square domain, 200 m on edge with a centrally located injection well. Constant pressure conditions are applied at the external boundary and fluid is injected at an overpressure of 1 MPa, 30°C cooler than ambient at the central wellbore. Quarter symmetry of the problem is used to represent a 10 * 10 mesh of equal sized elements. Material properties are those representative of a fractured granite rock mass. Details are recorded in Table 1.

Temperature dependent changes in fissure apertures modify the flow regime in a transient manner by influencing the permeability distribution within the domain. The sequence of changes in pressure distribution occasioned as cool fluid initially quenches the rock mass closest to the injection point and spreads radially outwards is illustrated in Figs 5a through 5e. A time interval of 4.16 h separates successive frames with the influence of permeability enhancement being expressed through a reduction in pressure gradient close to the wellbore. The parameter driving the change in pressure distribution is the advected fluid temperature, the temporal and spatial distribution of which is illustrated in Figs 6a through 6e at time increments of 4.16 h each. Apparent, especially in Figs 6b and 6c, are isolated areas of overshoot generated from the poor conditioning of even the upwind-weighted equations used in the present formulation. This overshoot is restricted to a maximum value of 10% of the initial temperature differential and is removed in successive time frames.

Table 1. Example parameters

| Symbol | Description | Case one Magnitude | Case two Magnitude | Units |
|---|---|---|---|---|
| $\sigma_{11}, \sigma_{22}, \sigma_{12}$ | Initial stresses | 0.3, 0.3, 0.2 | 52.5, 52.5, 20 | MPa |
| $\Delta P_f$ | Wellbore fluid pressure (above ambient) | +1.0 | +10.0 | MPa |
| $\Delta T_f$ | Injection temperature (relative to ambient) | −30 | −20 | degrees, C |
| $s$ | Joint spacing | 1.0 | 10.0 | m |
| $\rho_s$ | Solid density | 2627 | | kg/m$^3$ |
| $\nu$ | Poisson ratio | 0.22 | | — |
| $E$ | Deformation modulus | $58 \times 10^3$ | | MPa |
| $c_s$ | Specific heat capacity (solid) | 918 | | J/kg°C |
| $\alpha_s$ | Coef. of thermal expansion (solid) | $7.42 \times 10^{-6}$ | | /°C |
| $D_s$ | Thermal conductivity (solid) | 9770 | | J/hm°C |
| $k_n$ | Joint normal stiffness | $10^5$ | | MPa/m |
| $k_s$ | Joint shear stiffness | $5 \times 10^4$ | | MPa/m |
| $\phi_b$ | Joint friction angle | 40 | | degrees |
| $\phi_d$ | Joint dilatancy angle | 5 | | degrees |
| $\rho_f$ | Fluid density | 1000 | | kg/m$^3$ |
| $c_f$ | Specific heat capacity (fluid) | 4187 | | J/kg°C |
| $D_f$ | Thermal conductivity (fluid) | 2262 | | J/hm°C |
| $\beta_f$ | Fluid compressibility | $0.4239 \times 10^{-3}$ | | MPa$^{-1}$ |
| $\nu_f$ | Fluid kinematic viscosity | 0.0029 | | m$^2$/h |
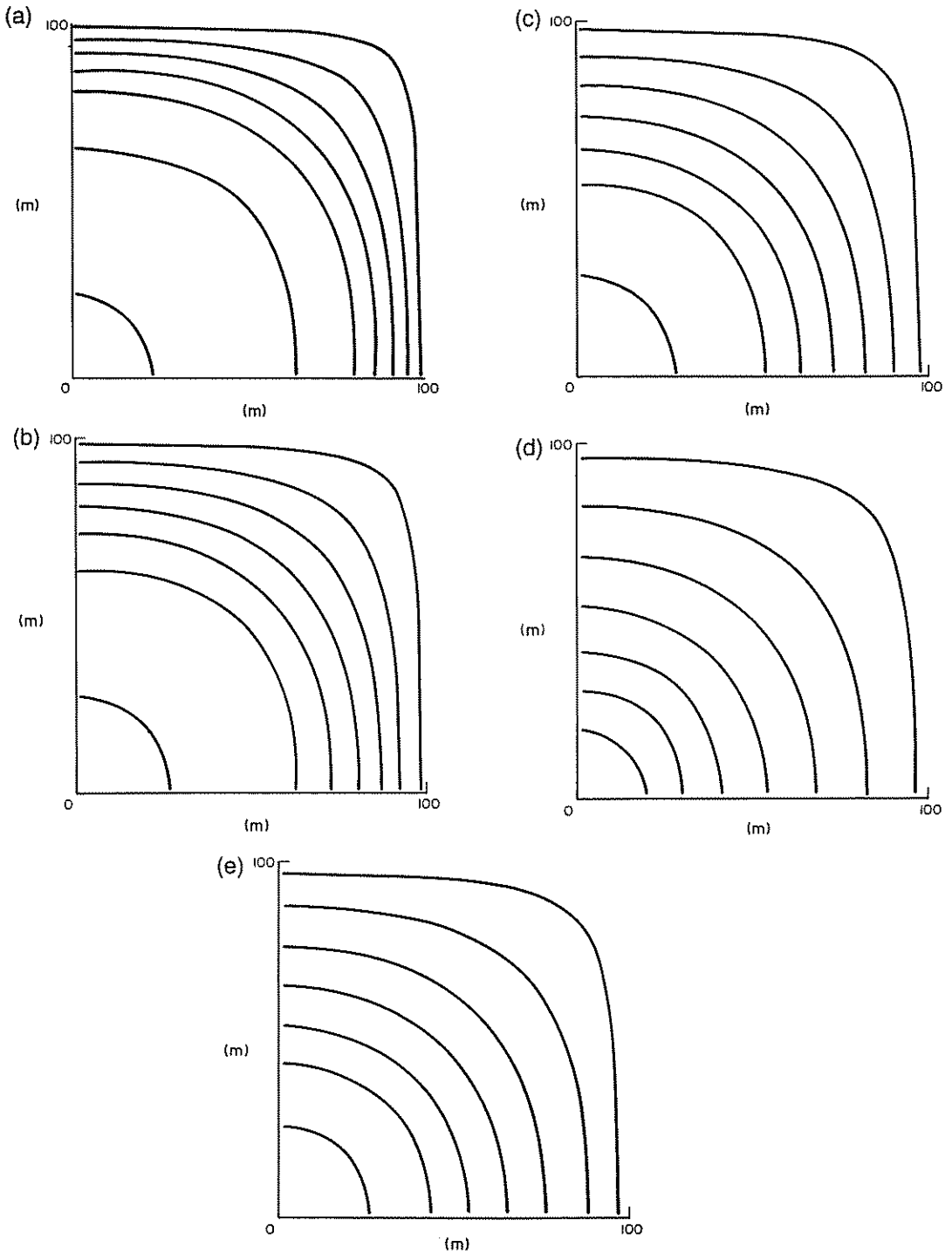
Fig. 5. Temporal change in fluid pressure distribution for injection into a square domain (Case one). Respective contour levels are at $P/\Delta P = 0.95, 0.80, 0.65, 0.50, 0.35, 0.20, 0.05$.

|  |  |
|---|---|
| (a) Time = 4.15 h | (c) Time = 12.45 h |
| (b) Time = 8.30 h | (d) Time = 16.60 h |
| (e) Time = 20.75 h | |

*D. Elsworth and J. Xiang*
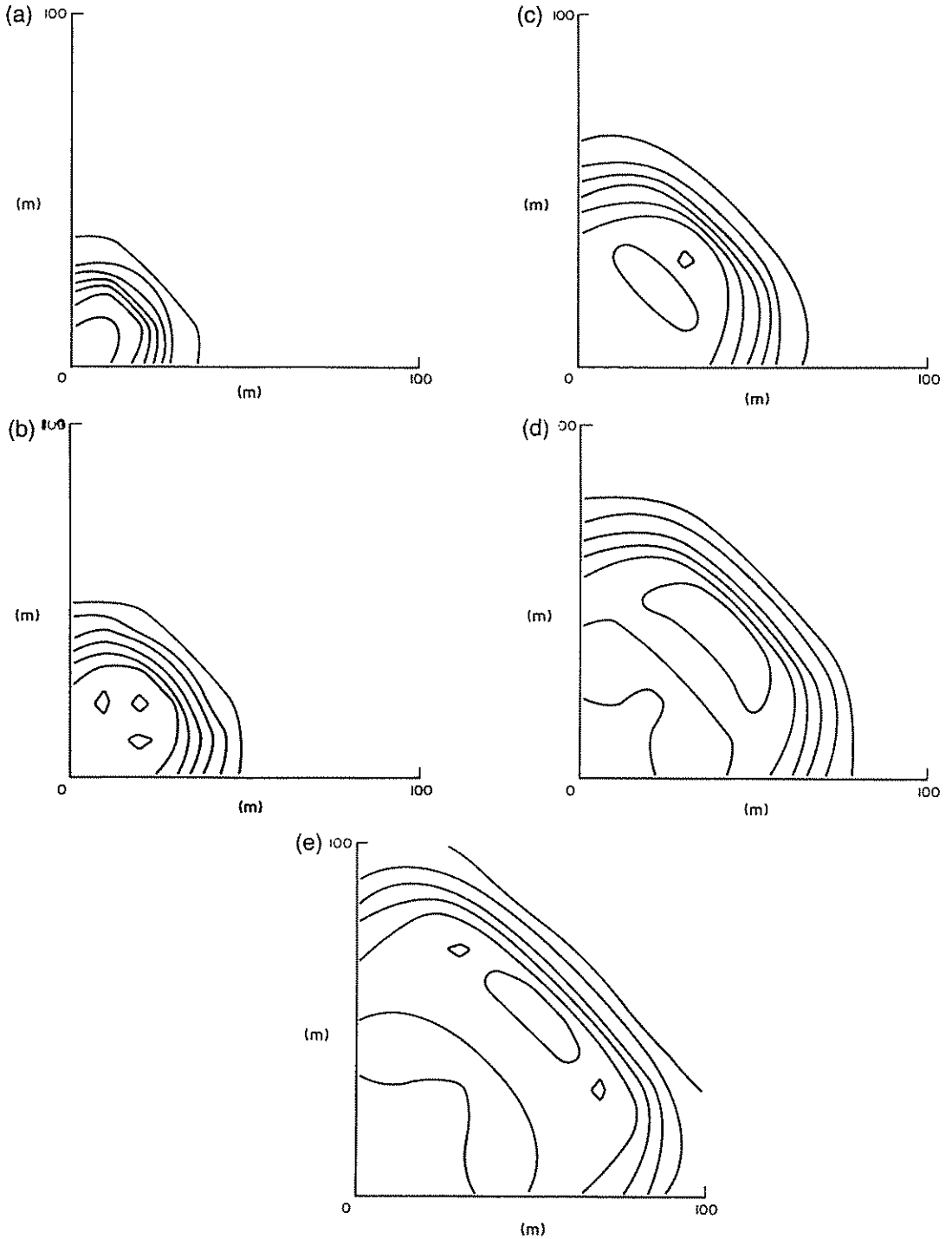


Fig. 6. Temporal change in fluid temperature distribution for injection into a square domain (Case one). Respective contour levels are at $T/\Delta T = 0.93, 0.80, 0.63, 0.50, 0.33, 0.20, 0.03$.

(a) Time = 4.15 h          (c) Time = 12.45 h

(b) Time = 8.30 h          (d) Time = 16.60 h

(c) Time = 20.75 h

Where the 10 * 10 mesh is substituted by a 20 * 20 mesh, the extreme sensitivity of the analysis to discretization density is effectively illustrated. The results for fluid temperature distribution in a refined mesh comprising 400 elements for the same initial value problem is illustrated in the contour plot of Fig. 7 at a time of 20.8 h. Comparison of Figs 6e and 7 illustrates the twofold influence of accurate description of permeability variation and equation stability on determining the location of the thermal front. Since permeability is assumed constant within individual elements, the density of discretization holds an important influence over the nonlinear solution of the problem. Of equal consequence in solving the system of equations, however, is the attendant stability for high values of Peclet number. By halving the edge dimension of all elements within the mesh, the local elemental Peclet number, as defined in equation (46), is also halved. This presents improved stability characteristics and reduced overshoot and undershoot. Reduction in the Peclet number also reduces the required magnitude of the upwinding coefficient ($a$) and may be a contributing factor further explaining the lag of the front in the case of the refined mesh. Of course, the increased precision is not gained without some computational penalty. Since the computational effort expended in solving the system of equations is proportional to the number of equations raised to the power three, quadrupling the number of equations increases the computational effort by a factor of 64.

The distribution of aperture enhancement within the section is illustrated in Fig. 8 after a time of 4.2 h. Large aperture changes are concentrated close to the injection point where the influence of temperature is greatest. Also apparent within the figure is the influence of the approximately radial pressure distribution on increasing apertures within the rock mass.

*Case two*

As an example of further application, results for a typical simultaneous injection-withdrawal stimulation are illustrated for the 400 × 300 m half symmetry section of Fig. 9. Physical parameters pertaining to the system are given in Table 1. The development of the fluid pressure distribution in the initially homogeneous formation is illustrated after 5.6 h in Fig. 10. The asymmetry of the flow system is readily apparent despite the symmetry of applied boundary conditions. This asymmetry is conditioned by the spatial distribution of permeability enhancement within the section as illustrated in Fig. 11. Permeability is increased immediately surrounding the injection point as a result of the mixed interaction of thermal and fluid pressure effects. The converse is true surrounding the withdrawal point where reduction in fluid
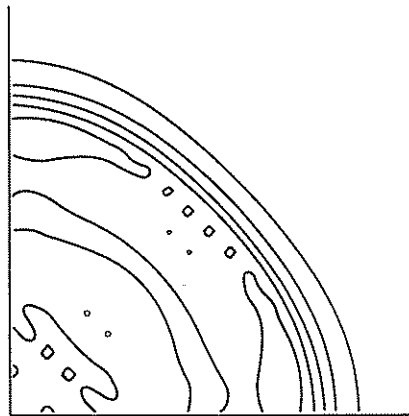


Fig. 7. Temperature distribution for a refined mesh (20 * 20) at time $t = 20.75$ h (Case one). Respective contour levels are at $T/\Delta T = 0.93, 0.80, 0.63, 0.50, 0.33, 0.20, 0.03$.
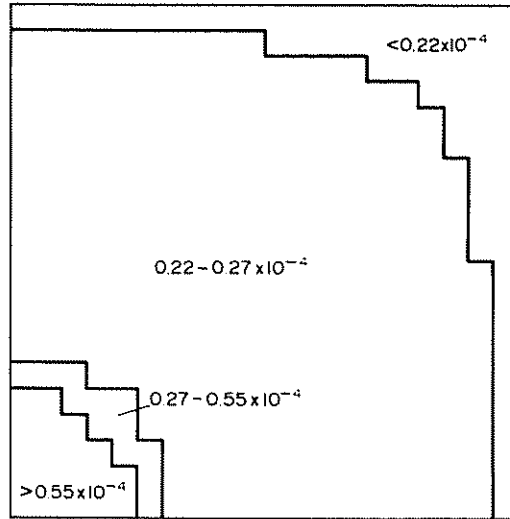
Fig. 8. Distribution of joint apertures at time $t = 4.15$ h (Case one). All apertures in metres.
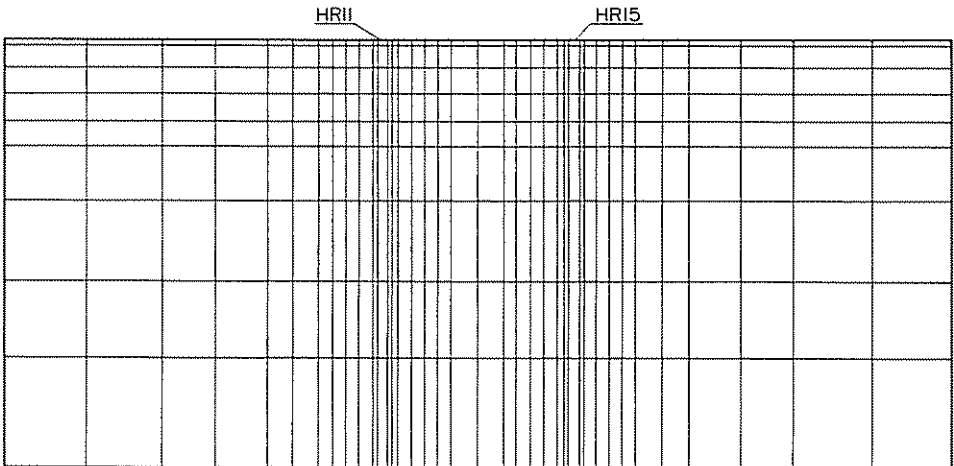


Fig. 9. Finite element mesh for simultaneous injection-withdrawal stimulation (Case two).
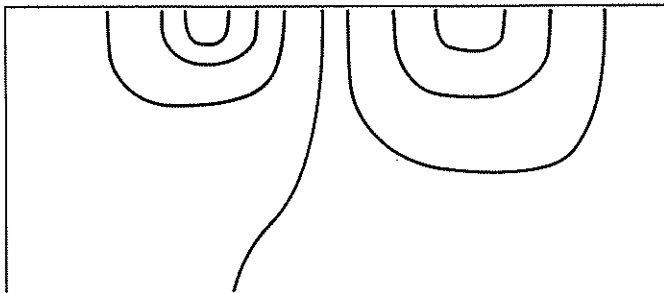


Fig. 10. Fluid pressure distribution for simultaneous injection-withdrawal at time $t = 5.6$ h (Case two). Respective contour levels are at $P/\Delta P = 0.95, 0.80, 0.65, 0.50, 0.35, 0.20, 0.05$.
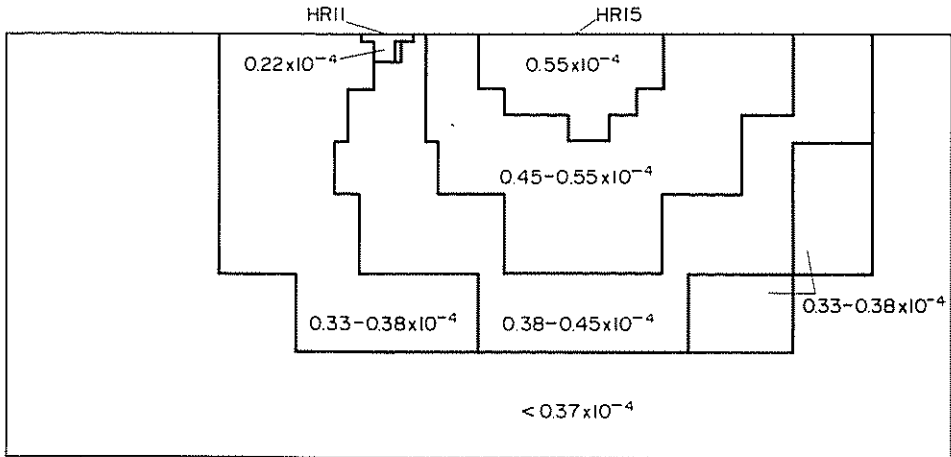
Fig. 11. Distribution of joint apertures at time $t = 5.6$ h (Case two). All apertures in metres.

pressures from the ambient state has induced fissure closure. It is this distribution of permeabilities throughout the domain that exercises a major control on the resulting time sequence of pressure changes and resulting flow rates and impedances through the fractured medium.

## CONCLUSIONS

The proposed model introduces some assumptions that allow solution of thermal transport problems in complex nonlinear geologic formations. The key assumption is that a macroscopic control volume must be considered to fully contain the same specified number of rock blocks. Subject to the validity of this requirement, the proposed solution scheme offers considerable utility in that nodal displacements and temperature distribution within the solid phase are treated as redundant parameters although their effects are intrinsically accommodated.

Assuming full lateral restraint, no attempt is made to solve for stress equilibrium explicitly since displacement degrees of freedom are deliberately made redundant. Any solution will therefore satisfy the compatibility, constitutive and boundary condition constraints of elasticity but violate equilibrium. Compatibility is enforced between adjacent elements and within individual elements. Zero displacement external boundary conditions are clearly satisfied as are the shear failure and compliance constitutive relationships within elements. Local equilibrium between adjacent rock blocks and joints within a single element is satisfied although inter-element equilibrium is violated.

The assumptions made in enforcing full lateral restraint are most readily appreciated against the framework of transient hydrogeologic analysis. The concept of storativity, invoked to quantify fluid volume released from storage under a change in fluid pressure, fails to satisfy either local equilibrium or compatibility. Nonetheless, storativity concepts have provided, for many decades, a satisfactory solution in the quantification of hydrologic analyses.

The elastic constitutive laws for the material are satisfied along with compatibility and boundary conditions for the solid phase. The only constraint violated through the assumption of full lateral restraint is that of local equilibrium between adjacent elements. All requirements for conservation of mass and energy applicable to the flow system are met on a transient basis.

Idealization of the rock volume as an assemblage of spherical blocks is used to cast the problem as tractable. This idealization maintains an equivalence between the energy content of the real and idealized solid components providing the solid volumes are equivalent as mandated

in equation (23). Displacements within the blocks are evaluated from a spherical analogue which maintains compatibility, in an elastic sense, throughout the deforming sphere and requires that surface deformations are consistent with heat loss at the boundary. However, although reasonable, the behavior does not directly address the thermal distribution and resulting deformation field within the real prismatic blocks. Errors precipitated in this manner are anticipated to be of low order, only.

The determination of block surface displacements and flux magnitudes requires the evaluation of an infinite exponential series. This individual computation within the solution procedure comprises a significant portion of the overall effort and requires special storage requirements for the antecedent magnitudes of parameters from the series. This burden becomes particularly onerous as the block size increases or as the thermal diffusivity decreases. This complication may be considerably eased if a quasi-steady approximation is used to represent heat flow from the individual blocks, requiring a constant temperature distribution throughout.

Dependent to some degree on the parameters chosen, the problem is intensely nonlinear. This nonlinearity exacerbates the intrinsic stability problems associated with numerical solution of advection dominated flows. Upwind-weighting of the solution has minimized this facet as far as appears reasonable.

## REFERENCES

Bear, J. (1972) *Dynamics of Fluids in Porous Media*. Elsevier, New York, 764 pp.

Bibby, R. (1981) Mass transport of solutes in dual porosity media. *Water Resour. Res.* **17**(4), 1075–1081.

Boley, B. A. and Weiner, J. H. (1960) *Theory of Thermal Stress*. John Wiley, New York.

Brekke, T. L., Noorishad, J., Witherspoon, P. A. and Maini, Y. N. T. (1972) Coupled stress and flow analysis of fractured dam foundations and rock slopes. *Proc. Symp. Percolation Through Fissured Rock*, Stuttgart T4-J, pp. 1–7.

Carslaw, H. S. and Jaeger, J. C. (1959) *Conduction of Heat in Solids*. Second Edition, Oxford University Press.

Christie, I., Griffiths, D. F., Mitchell, A. R. and Zienkiewicz, O. C. (1976) Finite element methods for second order differential equations with significant first derivatives. *Int. J. Num. Meth. Eng.* **10**, 1389–1396.

Elsworth, D. and Goodman, R. E. (1985) Characterization of rock fissure hydraulic conductivity using idealized wall roughness profiles. *Int. J. Rock Mech. Min. Sci. Geomech. Abstr.* **23**(3), 233–244.

Fairhurst, C. (1964) Measurement of in-situ rock stresses, with particular reference to hydraulic fracturing. *Rock Mech. Eng. Geol.* **2**, 3 & 4, 129–147.

Huyakorn, P. S., Lester, B. H. and Faust, C. R. (1983) Finite element techniques for modeling groundwater flow in fractured aquifers. *Water Resour. Res.* **19**(4), 1019–1035.

Murphy, H. (1982) Hot dry rock reservoir development and testing in the U.S.A. *Proc. 1st Japan–U.S. Seminar on Hydraulic Fracturing and Geothermal Energy*, Martinus Nijhoff, pp. 33–58.

Nemat-Nasser, S. (1982) Thermally induced cracks and heat extraction from hot dry rocks. *Proc. 1st Japan–U.S. Seminar on Hydraulic Fracturing and Geothermal Energy*, Martinus Nijhoff, pp. 11–31.

Noorishad, J. and Mehran, M. (1982) An upstream finite element method for solution of transient transport equation in fractured porous media. *Water Resour. Res.* **18**(3), 588–596.

Noorishad, J., Tsang, C. F. and Witherspoon, P. A. (1984) Coupled thermal-hydraulic-mechanical phenomena in saturated fractured porous rocks: Numerical approach. *J. geophys. Res.* **89**, B12, 10265–10373.

Pine, R. J. and Cundall, P. A. (1985) Applications of the fluid-rock interaction program (FRIP) to the modelling of hot dry rock geothermal energy systems. *Proc. Int. Symp. Fundamentals of Rock Joints*, Bjorkliden, pp. 293–302.

## APPENDIX I

The elemental matrices for a four noded, upwind-weighted element are:

$$\mathbf{D} = \int_{\Omega} \bar{\mathbf{W}}^{\mathrm{T}}(\mathrm{D}_f/\phi)\bar{\mathbf{N}}\, d\Omega$$

$$\mathbf{E} = \int_{\Omega} \rho_f c_f (q_f/\phi)_i \bar{\mathbf{W}}^T \mathbf{N} \, d\Omega$$

$$\mathbf{F} = \rho_f c_f \int_{\Omega} \mathbf{N}^T \mathbf{N} \, d\Omega$$

$$\mathbf{G} = \int_{\Omega} \mathbf{W}^T \mathbf{N} \, d\Omega$$

$$\mathbf{K} = \int_{\Omega} \frac{1}{\gamma_f} \bar{\mathbf{N}}^T \mathbf{K}_f \bar{\mathbf{N}} \, d\Omega$$

$$\mathbf{S} = \int_{\Omega} \phi \beta_l \mathbf{N}^T \mathbf{N} \, d\Omega$$

$$\mathbf{H} = \int_{\Omega} \phi a_f \mathbf{N}^T \mathbf{N} \, d\Omega$$

$$f_1(\eta, \alpha) = 1 - \eta + 3\alpha(\eta^2 - \eta)$$
$$f_2(\eta, \alpha) = \eta - 3\alpha(\eta^2 - \eta)$$
$$0 < x < h; \quad 0 < y < b$$

$$W_1 = f_1\left(\frac{x}{h}, \alpha_1\right) f_1\left(\frac{y}{b}, \beta_2\right); \quad N_1 = f_1\left(\frac{x}{h}, 0\right) f_1\left(\frac{y}{b}, 0\right)$$

$$W_2 = f_2\left(\frac{x}{h}, \alpha_1\right) f_1\left(\frac{y}{b}, \beta_1\right); \quad N_2 = f_2\left(\frac{x}{h}, 0\right) f_1\left(\frac{y}{b}, 0\right)$$

$$W_3 = f_2\left(\frac{x}{h}, \alpha_2\right) f_2\left(\frac{y}{b}, \beta_1\right); \quad N_3 = f_2\left(\frac{x}{h}, 0\right) f_2\left(\frac{y}{b}, 0\right)$$

$$W_4 = f_1\left(\frac{x}{h}, \alpha_2\right) f_2\left(\frac{y}{b}, \beta_2\right); \quad N_4 = f_1\left(\frac{x}{h}, 0\right) f_2\left(\frac{y}{b}, 0\right)$$

with $\quad \bar{\mathbf{W}} = \left[\frac{\partial}{\partial x}; \frac{\partial}{\partial y}\right]^T \mathbf{W}; \quad \bar{\mathbf{N}} = \left[\frac{\partial}{\partial x}; \frac{\partial}{\partial y}\right]^T N$

and $\quad 0 < |\alpha| < 1.0$